

# Numerical Algorithms for Partially Segregated Elliptic Systems

**Farid Bozorgnia**

Department of Mathematics  
New Uzbekistan University  
Tashkent, Uzbekistan  
drfaridba@gmail.com

**Avetik Arakelyan**

Institute of Mathematics, NAS of Armenia  
Yerevan State University  
Yerevan, Armenia  
avetik.arakelyan@ysu.am

**Vyacheslav Kungurtsev**

Department of Computer Science  
Czech Technical University in Prague, Faculty  
of Electrical Engineering  
Prague, Czech Republic  
vyacheslav.kungurtsev@fel.cvut.cz

**Jan Valdman**

Department of Decision-Making Theory  
UTIA CAS  
Prague, Czech Republic  
jan.valdman@utia.cas.cz

**ABSTRACT.** We develop numerical methods for elliptic systems governed by partial segregation constraints, in which three nonnegative components are required to have a vanishing pointwise product throughout the domain. This constraint enforces that at least one component must be zero at every spatial location, leading to a highly nonconvex admissible set that prevents the use of standard convex optimization techniques. We propose two complementary computational frameworks. The first is a strong-competition penalty method, solved via damped Gauss–Seidel/Picard iterations with a continuation strategy on the penalty parameter, for which we establish compactness results, Lipschitz estimates, and interior exponential improvement in the strong-competition regime. The second is a projected gradient method, together with an accelerated variant, that exploits an explicit pointwise projection onto the three-phase segregation set. Numerical experiments on a suite of benchmark boundary configurations confirm that both algorithms resolve segregated phase patterns.

## CONTENTS

1. Introduction	2
2. Mathematical Background and Previous Works	3
3. Proposed Numerical Constrained Optimization Algorithms	5
3.1. Penalization Method	5
Jacobi/Picard map $T$	10
Gauss–Seidel map $G$	11
3.2. Projected Gradient Method.	17
4. Simulations	20
5. Conclusion and Impact	25
References	26

## 1. INTRODUCTION

In recent decades, there has been considerable interest in the study of spatial segregation phenomena arising in reaction–diffusion systems. In particular, the existence of spatially inhomogeneous solutions for Lotka–Volterra–type competition models involving two or more interacting species has been extensively investigated (see [29, 14, 31, 32, 15, 27]). These systems lead to pairwise segregated problems, where solutions satisfy  $u_i \cdot u_j = 0$  for  $i \neq j$  (discussed in Section 2), lead to an important class of multi-phase free boundary problems, which capture the competition and coexistence dynamics among different components. These problems have gained interest due to their significant applications in various branches of applied mathematics. To see the diversity of applications, we refer to [1, 8, 9, 4] and the references therein.

In this paper, we investigate numerical schemes for approximating the solutions of a class of elliptic systems that describe competitive interactions among multiple components  $u_1, \dots, u_m$ , where each  $u_i: \Omega \rightarrow [0, \infty)$  represents the density (or concentration) of the  $i$ -th species defined on a bounded domain  $\Omega \subset \mathbb{R}^d$ ,  $d = 2$  or  $3$ , subject to the segregation constraint

$$\prod_{i=1}^m u_i(x) = 0,$$

which enforces that at least one component must vanish at each spatial location. This constraint leads to a natural spatial partition of the domain into regions dominated by distinct components. To the best of our knowledge, the numerical approximation of partially segregated elliptic systems has not been explored in the existing literature, which serves as a primary motivation for this work.

Such systems arise in models of multi-component Bose–Einstein condensates and other physical or biological systems involving strong competition between species. Also, this system and the limiting case appear in the theory of flames and are related to a model called the Burke–Schumann approximation. In comparison, several theoretical studies have explored the qualitative properties and asymptotic limits of these models (e.g., [26, 25, 7, 6]), but our focus here is entirely numerical. We develop computational schemes to approximate segregated equilibrium configurations efficiently.

The optimization of functionals subject to nonconvex constraints represents one of the most challenging problems in computational mathematics, where classical convex optimization theory provides limited guidance and standard numerical algorithms often fail to converge or converge to poor local optima. In [17], a number of variational problems with nonconvex constraints were found to have multiple local minima. Moreover, in the case considered in this work, the nonconvex constraint is irregular, that is, Robinson’s Constraint Qualification does not hold for any feasible point of the segregation constraint, invalidating the standard theory for establishing primal–dual first order necessary optimality conditions as a target for computational optimization [18]. A detailed mathematical study of optimality conditions is beyond the scope of this paper.

Traditional numerical methods for segregation problems often struggle with the inherent stiffness and non-smoothness of the solutions. Our main contributions can be summarized as follows. We implement a variety of optimization-based algorithms: penalty methods and projected gradient flows.

The remainder of this paper is structured as follows. Section 2 establishes the mathematical framework and reviews relevant theoretical results from the segregation literature. Section 3 presents our algorithmic developments, including detailed descriptions of each method and implementation considerations. Finally, Section 4 discusses numerical experiments.

## 2. MATHEMATICAL BACKGROUND AND PREVIOUS WORKS

Consider minimizing the following Dirichlet energy

$$E(U) = \int_{\Omega} \sum_{i=1}^m |\nabla u_i(x)|^2 dx \quad (1)$$

over the non-convex set

$$S = \left\{ (u_1, \dots, u_m) : u_i \in H^1(\Omega), u_i \geq 0, \prod_{i=1}^m u_i(x) = 0, u_i|_{\partial\Omega} = \phi_i \right\}. \quad (2)$$

**Assumption 2.1.** *The boundary data  $\phi_i$  are non-negative  $C^{1,\alpha}$  functions satisfying the segregation condition*

$$\prod_{i=1}^m \phi_i = 0 \quad \text{on } \partial\Omega.$$

A related class that bears certain similarities to the problem considered here is the adjacent (or pairwise) segregation model. The pairwise segregation model has been extensively studied in the literature. Segregation phenomena in elliptic systems are classically modeled by strongly competing reaction–diffusion systems of the type

$$\begin{cases} -\Delta u_i + \frac{1}{\varepsilon} u_i \sum_{j \neq i} u_j^2 = 0 & \text{in } \Omega, \\ u_i \geq 0, \quad u_i|_{\partial\Omega} = \phi_i, & i = 1, \dots, m, \end{cases} \quad (3)$$

with  $\varepsilon > 0$  a small competition parameter. As  $\varepsilon \rightarrow 0$ , the solutions  $(u_1, \dots, u_m)$  segregate, in the sense that

$$u_i(x) u_j(x) = 0 \quad \text{a.e. in } \Omega, \quad i \neq j,$$

so that at most one component is active at each spatial point. Functions in the admissible class thus describe the limiting configurations

$$\mathcal{S}_1 := \left\{ U = (u_1, \dots, u_m) \in (H^1(\Omega))^m : u_i \geq 0, u_i u_j = 0 \ (i \neq j) \right\}.$$

The limiting solution of system (3) is the minimizer of the following

$$E(U) = \int_{\Omega} \sum_{i=1}^m |\nabla u_i|^2 dx \quad (4)$$

over the nonconvex set  $\mathcal{S}_1$  with prescribed boundary conditions. The present work treats the partial segregation problem both as a variational constraint model and the limit of a specific PDE model.

The rigorous asymptotic analysis of (3) as  $\varepsilon \rightarrow 0$  has been extensively studied in the literature. Seminal works by Caffarelli and Lin [10], and [24, 16] have established compactness, regularity of limiting interfaces, and the relation to optimal partition problems, see also [4].

**Definition 2.2.** Let  $U = (u_1, \dots, u_m)$  with  $u_i \geq 0$ . We distinguish two admissible classes:

- Pairwise segregation:

$$u_i u_j = 0 \quad \text{for all } i \neq j,$$

denoted by the admissible set  $\mathcal{S}_1$ .

- Partial segregation:

$$\prod_{i=1}^m u_i = 0,$$

denoted by the admissible set  $\mathcal{S}$ .

The main differences between these two notions are as follows:

- (1) Coexistence structure. Partial segregation requires that at each point  $x$  *at least one* component vanishes. Thus  $\mathcal{S}$  allows up to  $m - 1$  components to be simultaneously positive, whereas  $\mathcal{S}_1$  restricts each point to having at most *one* positive component.
- (2) Geometry of the admissible sets. The set  $\mathcal{S}_1$  is the finite union of mutually disjoint convex cones  $\bigcup_{i=1}^m \{u_j = 0 \text{ for all } j \neq i\}$ , so, at each point, exactly one species may survive. In contrast,  $\mathcal{S}$  has a highly overlapping structure; points may belong to multiple cones simultaneously (e.g. when two or more components vanish).
- (3) For  $m = 3$ , the vector  $(0.5, 0.3, 0)$  belongs to  $\mathcal{S}$  because at least one entry is zero, but it does *not* belong to  $\mathcal{S}_1$  since more than one component is positive.

From a computational perspective, the direct numerical solution of segregation problems presents several challenges. The penalty parameter  $\varepsilon$  must be chosen very small to approximate the segregation constraint, leading to severely ill-conditioned systems that challenge standard numerical methods. The segregation constraints define a nonconvex feasible region, rendering standard convex optimization techniques inapplicable. The non-convexity often results in multiple local solutions, posing challenges for solution selection and convergence to a global optimum.

These challenges have motivated the development of various computational approaches in the literature, including penalty methods that regularize the constraint violations, level-set and phase-field methods that represent interfaces implicitly [23, 3], and optimization-based approaches that systematically handle constraints through Lagrange multipliers and active set strategies [19].

Most existing numerical studies of diffusion systems with spatial segregation of Lotka–Volterra type focus primarily on two-component models, often restricted to one-dimensional domains. For instance, in [11], the analysis of new conditional symmetries and exact solutions is presented for the two-component diffusive Lotka–Volterra system, while in [12], a review and construction of exact solutions is likewise confined to the two-species case. Although such works provide insight into the underlying dynamics, they do not address the more challenging setting of multi-component systems in higher dimensions, where complex segregation patterns and interface structures arise; see also [22, 28, 13, 2].

The partial segregation set  $\mathcal{S}$  is geometrically much more complex than the pairwise set  $\mathcal{S}_1$ . In  $\mathcal{S}_1$  each point belongs to one of  $m$  *disjoint* convex cones (exactly one active component). In contrast,  $\mathcal{S}$  contains many *overlapping* cones, since any number of components may vanish simultaneously. This produces a far larger set of feasible switching patterns and a highly singular constraint, because the map  $U \mapsto \prod_i u_i$  has a degenerate Jacobian on every set where some

$u_i = 0$ . Penalty terms such as  $(u_1 u_2 u_3)^2$  are more ill-conditioned than pairwise terms  $u_i u_j$ . These make the partial segregation problem numerically more delicate and justify the need for specialized algorithms.

### 3. PROPOSED NUMERICAL CONSTRAINED OPTIMIZATION ALGORITHMS

Optimization problems constrained over nonconvex sets frequently arise in applied mathematics, physics, and machine learning, where one aims to balance competing effects under nonlinear or geometric constraints [21, 20]. As we mentioned in the previous section, these problems are challenging due to the possible non-uniqueness of solutions, the absence of convexity, and the sensitivity of numerical schemes to initial data and parameter choices. Developing stable and efficient numerical algorithms that can effectively address these difficulties is therefore of fundamental importance. In this section, we develop and analyze two numerical algorithms for solving the constrained optimization problem defined over the nonconvex set  $S$ . Each algorithm seeks to approximate a stationary point of the constrained functional by iteratively minimizing an energy or Lagrangian under constraint consistency. In this work, we present two approaches.

The first scheme is the Penalization Method, which introduces a penalty term to regularize constraint violations, transforming the constrained problem into a sequence of unconstrained problems. This approach is conceptually the simplest and provides insight into the structure of the feasible region. Next, we implement the Projected Gradient Method, which performs a gradient descent step followed by orthogonal projection onto  $S$ . It is straightforward to implement and computationally efficient for problems with simple geometric constraints.

**3.1. Penalization Method.** We penalize the constraint  $(u_1 u_2 u_3) = 0$  as:

$$E^\varepsilon(U) = \int_{\Omega} \sum_{i=1}^3 |\nabla u_i|^2 dx + \frac{1}{\varepsilon} \int_{\Omega} (u_1 u_2 u_3)^2 dx, \quad \varepsilon > 0, \quad (5)$$

with only the conditions  $u_i|_{\partial\Omega} = \phi_i$  imposed a priori. As  $\varepsilon \rightarrow 0$ , any limit point of minimizers of  $E^\varepsilon$  satisfies the segregation constraint. Note that, at this stage, we do not claim that the limit minimizers also minimize (1)-(2).

**Proposition 3.1.** *Let  $(u_1^\varepsilon, u_2^\varepsilon, u_3^\varepsilon)$  be minimizer to the penalized energy*

$$E^\varepsilon(u) = \int_{\Omega} \sum_{i=1}^3 |\nabla u_i|^2 dx + \frac{1}{\varepsilon} \int_{\Omega} (u_1 u_2 u_3)^2 dx$$

*subject to  $u_i^\varepsilon|_{\partial\Omega} = \phi_i$  and  $u_i^\varepsilon \geq 0$ . Then  $u_i^\varepsilon \rightharpoonup \bar{u}_i$  weakly in  $H^1(\Omega)$  up to a subsequence for  $i = 1, 2, 3$ . Moreover  $(\bar{u}_1, \bar{u}_2, \bar{u}_3) \in S$ .*

*Proof.* Let  $u^* = (u_1^*, u_2^*, u_3^*) \in S$  be a minimizer of the constrained problem

$$\min_{u \in S} E(u) = \min_{u \in S} \int_{\Omega} \sum_{i=1}^3 |\nabla u_i|^2 dx.$$

Such a minimizer  $u^*$  exists by standard direct methods in the calculus of variations. Since  $u^*$  satisfies the segregation constraint  $\prod_i u_i^* = 0$  a.e., the penalty term vanishes when we use  $u^*$  as a competitor for the penalized problem. We get

$$\begin{aligned} E^\varepsilon(u^\varepsilon) &\leq E^\varepsilon(u^*) \\ &= \int_\Omega \sum_{i=1}^3 |\nabla u_i^*|^2 dx + \frac{1}{\varepsilon} \int_\Omega \underbrace{(u_1^* u_2^* u_3^*)^2}_{=0 \text{ a.e.}} dx \\ &= E(u^*) < +\infty. \end{aligned}$$

Therefore,  $\sup_{\varepsilon>0} E^\varepsilon(u^\varepsilon) \leq E(u^*) < +\infty$ . We use  $E(u^*)$  as our bound because  $u^*$  satisfies the segregation constraint and thus is a valid competitor for all  $\varepsilon > 0$ . From the energy we have

$$\frac{1}{\varepsilon} \int_\Omega (u_1^\varepsilon u_2^\varepsilon u_3^\varepsilon)^2 dx = E^\varepsilon(u^\varepsilon) - \int_\Omega \sum_i |\nabla u_i^\varepsilon|^2 dx \leq E(u^*).$$

Therefore,

$$\left\| \prod_i u_i^\varepsilon \right\|_{L^2}^2 \leq \varepsilon \cdot E(u^*) \implies \left\| \prod_i u_i^\varepsilon \right\|_{L^2} \leq \sqrt{\varepsilon \cdot E(u^*)} = C\sqrt{\varepsilon}. \quad (6)$$

From the first part,  $u^\varepsilon$  is bounded in  $H^1(\Omega)^3$ . By the Rellich-Kondrachov compactness theorem, there exists a subsequence with

$$u_i^{\varepsilon_k} \rightarrow \bar{u}_i \quad \text{strongly in } L^2(\Omega), \quad u_i^{\varepsilon_k} \rightharpoonup \bar{u}_i \quad \text{weakly in } H^1(\Omega).$$

Due to (6) we conclude  $\|\prod_i u_i^{\varepsilon_k}\|_{L^2} \rightarrow 0$ , hence  $\prod_i \bar{u}_i = 0$ , which implies  $(\bar{u}_1, \bar{u}_2, \bar{u}_3) \in S$ .  $\square$

**Remark 3.2.** It is noteworthy that due to recent works [26, 25], the vector  $(\bar{u}_1, \bar{u}_2, \bar{u}_3) \in S$  is in fact a minimizer to (1)-(2).

Formally differentiating  $E^\varepsilon$  yields, for  $i = 1, 2, 3$ ,

$$-\Delta u_i^\varepsilon + \frac{1}{\varepsilon} u_i^\varepsilon (u_j^\varepsilon u_k^\varepsilon)^2 = 0 \quad \text{in } \Omega, \quad u_i^\varepsilon|_{\partial\Omega} = \phi_i, \quad (7)$$

where  $\{i, j, k\} = \{1, 2, 3\}$ . Equivalently, given  $u_j^\varepsilon, u_k^\varepsilon$ , the  $i$ -th equation is linear in  $u_i^\varepsilon$ :

$$-\Delta u_i^\varepsilon + c_i^\varepsilon(x) u_i^\varepsilon = 0, \quad c_i^\varepsilon(x) := \frac{1}{\varepsilon} (u_j^\varepsilon u_k^\varepsilon)^2 \geq 0. \quad (8)$$

In the *penalized* problem (7), we do *not* impose  $u_i^\varepsilon \geq 0$  explicitly, and positivity follows from the maximum principle.

As  $\varepsilon \rightarrow 0$ , one recovers a segregated state. However, because of the challenging regularity properties of the original problem, theoretical guarantees of optimality as far as standard first order conditions cannot be constructed. Consideration of notions of stationarity specific to complementarity constraints on optimization over Banach spaces as presented in, e.g. [30], have not been derived for this or other algorithms presented, to the best of the authors' knowledge, and would necessitate significant theoretical development.

Let  $\Omega \subset \mathbb{R}^n$  be a bounded Lipschitz domain and fix  $\varepsilon > 0$ . Assume boundary data  $\phi_i \in H^{1/2}(\partial\Omega) \cap L^\infty(\partial\Omega)$  with  $\phi_i \geq 0$  for  $i = 1, 2, 3$ . In the rest of the paper, we drop the dependence  $\varepsilon$  in  $u_i^\varepsilon$ , and we write  $u_i$ . Consider

$$\begin{cases} \Delta u_i = \frac{u_i}{\varepsilon} \prod_{j \neq i} u_j^2 & \text{in } \Omega, \\ u_i = \phi_i & \text{on } \partial\Omega, \end{cases} \quad i = 1, 2, 3. \quad (9)$$

Set

$$M := \max_{i=1,2,3} \|\phi_i\|_{L^\infty(\partial\Omega)}. \quad (10)$$

Let  $\lambda_D > 0$  be the first Dirichlet eigenvalue of  $-\Delta$  on  $\Omega$ :

$$\lambda_D := \inf_{w \in H_0^1(\Omega) \setminus \{0\}} \frac{\int_\Omega |\nabla w|^2 dx}{\int_\Omega |w|^2 dx}. \quad (11)$$

In particular,

$$\int_\Omega |\nabla w|^2 dx \geq \lambda_D \int_\Omega |w|^2 dx \quad \text{for all } w \in H_0^1(\Omega). \quad (12)$$

We repeatedly use the inequalities, valid whenever the indicated quantities lie in  $[-M, M]$ :

$$|a^2 - b^2| \leq 2M|a - b|, \quad |(ab)^2 - (cd)^2| \leq 2M^3(|a - c| + |b - d|). \quad (13)$$

We begin with the linear Dirichlet theory that will be used throughout: well-posedness and an  $H^1$  bound, a maximum principle, a comparison principle, and an  $L^2$  resolvent estimate.

**Lemma 3.3.** *Let  $q \in L^\infty(\Omega)$  with  $q \geq 0$  and let  $\phi \in H^{1/2}(\partial\Omega)$ . There exists a unique  $z \in H^1(\Omega)$  with trace  $z|_{\partial\Omega} = \phi$  such that*

$$-\Delta z + \frac{q}{\varepsilon} z = 0 \quad \text{in } \Omega. \quad (14)$$

Moreover,

$$\|z\|_{H^1(\Omega)} \leq C(\Omega) \left(1 + \frac{\|q\|_{L^\infty(\Omega)}}{\varepsilon}\right) \|\phi\|_{H^{1/2}(\partial\Omega)}. \quad (15)$$

*Proof.* Choose an extension  $\Phi \in H^1(\Omega)$  of  $\phi$  with  $\|\Phi\|_{H^1(\Omega)} \leq C(\Omega) \|\phi\|_{H^{1/2}(\partial\Omega)}$ . Write  $z = \Phi + w$  with  $w \in H_0^1(\Omega)$ . Then  $z$  satisfies (14) if and only if  $w$  satisfies, for all  $\psi \in H_0^1(\Omega)$ ,

$$\int_\Omega \nabla w \cdot \nabla \psi dx + \int_\Omega \frac{q}{\varepsilon} w \psi dx = - \int_\Omega \nabla \Phi \cdot \nabla \psi dx - \int_\Omega \frac{q}{\varepsilon} \Phi \psi dx.$$

The left-hand side is a coercive, continuous bilinear form on  $H_0^1(\Omega)$  (since  $q \geq 0$ ), hence by Lax–Milgram there exists a unique  $w \in H_0^1(\Omega)$ . Uniqueness of  $z$  follows.

Testing the identity with  $\psi = w$  and using Cauchy–Schwarz and Young’s inequality yields

$$\|\nabla w\|_{L^2}^2 + \int_\Omega \frac{q}{\varepsilon} w^2 \leq \frac{1}{2} \|\nabla w\|_{L^2}^2 + \frac{1}{2} \|\nabla \Phi\|_{L^2}^2 + \frac{1}{2} \int_\Omega \frac{q}{\varepsilon} w^2 + \frac{1}{2} \int_\Omega \frac{q}{\varepsilon} \Phi^2.$$

Hence

$$\|\nabla w\|_{L^2}^2 + \int_\Omega \frac{q}{\varepsilon} w^2 \leq \|\nabla \Phi\|_{L^2}^2 + \frac{\|q\|_{L^\infty}}{\varepsilon} \|\Phi\|_{L^2}^2 \leq C(\Omega) \left(1 + \frac{\|q\|_{L^\infty}}{\varepsilon}\right) \|\Phi\|_{H^1}^2.$$

By Poincaré,  $\|w\|_{L^2} \leq C(\Omega)\|\nabla w\|_{L^2}$ , so  $\|w\|_{H^1} \leq C(\Omega)\|\nabla w\|_{L^2}$ . Combining with the bound on  $\|\Phi\|_{H^1}$  yields (15).  $\square$

The next lemma states the weak maximum principle in the present setting, yielding uniform bounds from the boundary data.

**Lemma 3.4.** *Let  $q \in L^\infty(\Omega)$  with  $q \geq 0$  and let  $z \in H^1(\Omega)$  be a weak solution of*

$$-\Delta z + \frac{q}{\varepsilon}z = 0 \quad \text{in } \Omega$$

*with trace  $z|_{\partial\Omega} = \phi$ , where  $\phi \in H^{1/2}(\partial\Omega) \cap L^\infty(\partial\Omega)$  and  $\phi \geq 0$ . Then*

$$0 \leq z \leq \|\phi\|_{L^\infty(\partial\Omega)} \quad \text{a.e. in } \Omega.$$

*Proof.* Let  $m := \|\phi\|_{L^\infty(\partial\Omega)}$ . To show non-negativity, let  $z^- := (-z)^+ = \max\{-z, 0\} \in H^1(\Omega)$ . Since  $\phi \geq 0$ , the trace of  $z^-$  on  $\partial\Omega$  vanishes, hence  $z^- \in H_0^1(\Omega)$ . Testing the weak formulation by  $z^-$  gives

$$\int_{\Omega} |\nabla z^-|^2 dx + \int_{\Omega} \frac{q}{\varepsilon} (z^-)^2 dx = 0,$$

so  $z^- \equiv 0$  and therefore  $z \geq 0$  a.e.

Let  $w := (z - m)^+ \in H^1(\Omega)$ . Since the trace of  $z - m$  equals  $\phi - m \leq 0$  on  $\partial\Omega$ , we have  $w \in H_0^1(\Omega)$ . Testing by  $w$  yields

$$\int_{\Omega} |\nabla w|^2 dx + \int_{\Omega} \frac{q}{\varepsilon} w^2 dx = 0,$$

hence  $w \equiv 0$ , i.e.  $z \leq m$  a.e.  $\square$

We next compare solutions when the coefficients are ordered.

**Lemma 3.5.** *Let  $c_1, c_2 \in L^\infty(\Omega)$  satisfy  $0 \leq c_1 \leq c_2$  a.e. in  $\Omega$ . Let  $u, v \in H^1(\Omega)$  be weak solutions of*

$$-\Delta u + \frac{c_1}{\varepsilon}u = 0, \quad -\Delta v + \frac{c_2}{\varepsilon}v = 0 \quad \text{in } \Omega,$$

*with the same trace  $u|_{\partial\Omega} = v|_{\partial\Omega} = \phi$ , where  $\phi \in H^{1/2}(\partial\Omega) \cap L^\infty(\partial\Omega)$  and  $\phi \geq 0$ . Then  $u \geq v$  a.e. in  $\Omega$ .*

*Proof.* By Lemma 3.4, we have  $u \geq 0$  a.e. in  $\Omega$ . Let  $w := (v - u)^+ \in H^1(\Omega)$ . Since  $u$  and  $v$  have the same trace,  $w$  has zero trace on  $\partial\Omega$ , hence  $w \in H_0^1(\Omega)$ . Subtracting the two equations gives, in the weak sense,

$$-\Delta(v - u) + \frac{c_2}{\varepsilon}(v - u) = -\frac{c_2 - c_1}{\varepsilon}u \leq 0.$$

Testing by  $w$  and integrating by parts yields

$$\int_{\Omega} |\nabla w|^2 dx + \int_{\Omega} \frac{c_2}{\varepsilon} w^2 dx = - \int_{\Omega} \frac{c_2 - c_1}{\varepsilon} u w dx \leq 0.$$

Therefore  $w \equiv 0$ , i.e.  $v \leq u$  a.e.  $\square$

We finally record an  $L^2$  resolvent bound for the Dirichlet problem, which will be the key estimate for difference equations.

**Lemma 3.6.** *Let  $q \in L^\infty(\Omega)$  with  $q \geq 0$ , and let  $w \in H_0^1(\Omega)$  solve*

$$-\Delta w + \frac{q}{\varepsilon} w = f \quad \text{in } \Omega$$

*weakly, with  $f \in L^2(\Omega)$ . Then*

$$\|w\|_{L^2(\Omega)} \leq \frac{1}{\lambda_D} \|f\|_{L^2(\Omega)}.$$

*Proof.* Testing by  $w$  the equation  $-\Delta w + \frac{q}{\varepsilon} w = f$  we get

$$\int_{\Omega} |\nabla w|^2 dx + \int_{\Omega} \frac{q}{\varepsilon} w^2 dx = \int_{\Omega} f w dx \leq \|f\|_{L^2} \|w\|_{L^2}.$$

Using inequality (12) and dropping the nonnegative term  $\int_{\Omega} \frac{q}{\varepsilon} w^2$  leads to the desired result.  $\square$

The following three auxiliary lemmas are placed below because they will be used to refine interior estimates in the strong-competition regime.

**Lemma 3.7.** *Let  $q \in L^\infty(\Omega)$  satisfy  $q \geq 0$  a.e. in  $\Omega$ . Let  $z \in H^1(\Omega)$  be a weak solution of*

$$-\Delta z + \frac{q}{\varepsilon} z = 0 \quad \text{in } \Omega$$

*with boundary trace  $z|_{\partial\Omega} = \phi \in H^{1/2}(\partial\Omega) \cap L^\infty(\partial\Omega)$ . Fix open sets  $K_0 \Subset U \Subset \Omega$  and assume that*

$$q(x) \geq q_0 > 0 \quad \text{for a.e. } x \in U.$$

*Then there exist constants  $C = C(\Omega, U, K_0) > 0$  and  $c = c(\Omega, U, K_0) > 0$  such that*

$$\|z\|_{L^\infty(K_0)} \leq C \|\phi\|_{L^\infty(\partial\Omega)} \exp\left(-c \sqrt{\frac{q_0}{\varepsilon}}\right).$$

*Proof.* By Lemma 3.4 applied to  $\pm z$ , we have  $\|z\|_{L^\infty(\Omega)} \leq \|\phi\|_{L^\infty(\partial\Omega)}$ . Set  $d := \text{dist}(K_0, \partial U) > 0$  and fix  $x_0 \in K_0$  so that  $B_d(x_0) \subset U$ . Let  $m := \sqrt{q_0/\varepsilon}$  and let  $h = h_{m,d}$  be the (radial) solution of

$$-\Delta h + m^2 h = 0 \quad \text{in } B_d(x_0), \quad h = 1 \quad \text{on } \partial B_d(x_0).$$

Then  $0 < h \leq 1$  in  $B_d(x_0)$  and standard ODE/Bessel estimates imply

$$h(x_0) \leq C_1 e^{-md} \quad \text{for some } C_1 = C_1(n) > 0.$$

Since  $q \geq q_0$  a.e. in  $B_d(x_0)$ , we have

$$-\Delta h + \frac{q}{\varepsilon} h \geq -\Delta h + \frac{q_0}{\varepsilon} h = -\Delta h + m^2 h = 0 \quad \text{in } B_d(x_0).$$

Let  $M_\partial := \|z\|_{L^\infty(\partial B_d(x_0))}$  and set  $w := z - M_\partial h$ . Then  $w \leq 0$  on  $\partial B_d(x_0)$  and

$$-\Delta w + \frac{q}{\varepsilon} w = -\left(-\Delta(M_\partial h) + \frac{q}{\varepsilon}(M_\partial h)\right) \leq 0 \quad \text{in } B_d(x_0).$$

By the weak maximum principle,  $w \leq 0$  in  $B_d(x_0)$ , hence

$$|z(x_0)| \leq M_\partial h(x_0) \leq M_\partial C_1 e^{-md} \leq \|\phi\|_{L^\infty(\partial\Omega)} C_1 e^{-md}.$$

Taking the supremum over  $x_0 \in K_0$  yields the claimed estimate after absorbing  $d$  and  $C_1$  into constants  $C, c$  depending on  $(\Omega, U, K_0)$ .  $\square$

**Lemma 3.8.** *Assume that  $(u^\varepsilon)_{\varepsilon>0}$  is a family of variationally selected solutions of (9), for instance global minimizers (or local minimizers in the sense of [26]) of the energy*

$$E_\varepsilon(u) := \frac{1}{2} \sum_{i=1}^3 \int_{\Omega} |\nabla u_i|^2 dx + \frac{1}{2\varepsilon} \int_{\Omega} (u_1 u_2 u_3)^2 dx \quad (16)$$

among competitors with the same Dirichlet boundary traces  $(\phi_1, \phi_2, \phi_3)$ . Then for every compact set  $K_0 \Subset \Omega$  there exists a subsequence  $\varepsilon_k \downarrow 0$  such that

$$\int_{K_0} \frac{(u_1^{\varepsilon_k} u_2^{\varepsilon_k} u_3^{\varepsilon_k})^2}{\varepsilon_k} dx \longrightarrow 0 \quad \text{as } k \rightarrow \infty. \quad (17)$$

*Proof.* This follows from the  $\beta \rightarrow +\infty$  asymptotics for singularly perturbed segregation systems proved in [26]. Writing  $\beta := \varepsilon^{-1}$  and applying the corresponding interior estimate on any  $K_0 \Subset \Omega$  yields (17) along a subsequence.  $\square$

**Lemma 3.9** ([26]). *Assume that  $\Omega$  has  $C^1$  boundary and that the Dirichlet data  $(\phi_1, \phi_2, \phi_3)$  admit a nonnegative Lipschitz extension  $\psi = (\psi_1, \psi_2, \psi_3) \in \text{Lip}(\Omega)^3$  with  $\psi_i|_{\partial\Omega} = \phi_i$  and satisfying the partial segregation condition*

$$\psi_1 \psi_2 \psi_3 \equiv 0 \quad \text{in } \Omega.$$

Let  $u^\varepsilon$  be a family of (globally or locally) energy-minimizing solutions of (9) associated to (16) in the sense of [26] (equivalently, set  $\beta = \varepsilon^{-1}$  in their notation). Then there exists  $\bar{\nu} \in (0, 1)$  depending only on  $n$  such that, for every  $\alpha \in (0, \bar{\nu})$ ,

$$\|u^\varepsilon\|_{C^{0,\alpha}(\Omega)} \leq C \quad \text{with } C \text{ independent of } \varepsilon.$$

Moreover, along a subsequence  $\varepsilon_k \downarrow 0$  there exists a limit  $u = (u_1, u_2, u_3) \in H^1(\Omega)^3 \cap C^{0,\alpha}(\Omega)^3$  such that

$$u^{\varepsilon_k} \rightarrow u \quad \text{in } H^1(\Omega)^3 \text{ and in } C^{0,\alpha}(\Omega)^3 \text{ for every } \alpha \in (0, \bar{\nu}),$$

and the limiting profile satisfies

$$u_1 u_2 u_3 \equiv 0 \quad \text{a.e. in } \Omega, \quad \Delta u_i = 0 \quad \text{in } \{u_i > 0\} \quad (i = 1, 2, 3).$$

Define the Banach space  $X := (L^2(\Omega))^3$  with norm

$$\|u\|_X := \max_{i=1,2,3} \|u_i\|_{L^2(\Omega)}.$$

Define the closed convex set

$$K := \{u \in X : 0 \leq u_i \leq M \text{ a.e. in } \Omega, \quad i = 1, 2, 3\}.$$

**Jacobi/Picard map  $T$ .** For  $u = (u_1, u_2, u_3) \in K$ , define  $T(u) = v$  where  $v_i$  solves

$$\begin{cases} \Delta v_i = \frac{v_i}{\varepsilon} (u_j u_\ell)^2 & \text{in } \Omega, \\ v_i|_{\partial\Omega} = \phi_i, \end{cases} \quad \{i, j, \ell\} = \{1, 2, 3\}. \quad (18)$$

Equivalently,  $-\Delta v_i + \frac{(u_j u_\ell)^2}{\varepsilon} v_i = 0$ .

**Gauss–Seidel map  $G$ .** For  $u \in K$ , define  $G(u) = v$  sequentially by

$$\begin{cases} -\Delta v_1 + \frac{(u_2 u_3)^2}{\varepsilon} v_1 = 0, & v_1|_{\partial\Omega} = \phi_1, \\ -\Delta v_2 + \frac{u_3^2(u_1^2 + v_1^2)}{2\varepsilon} v_2 = 0, & v_2|_{\partial\Omega} = \phi_2, \\ -\Delta v_3 + \frac{(u_1 u_2)^2 + (v_1 v_2)^2}{2\varepsilon} v_3 = 0, & v_3|_{\partial\Omega} = \phi_3. \end{cases} \quad (19)$$

The next lemma shows that both fixed-point maps preserve the order interval  $K$ .

**Lemma 3.10.** *For every  $u \in K$ , one has  $T(u) \in K$  and  $G(u) \in K$ .*

*Proof.* All coefficients in (18) and (19) are nonnegative and bounded. By Lemma 3.4 applied componentwise, we obtain  $0 \leq v_i \leq \|\phi_i\|_{L^\infty(\partial\Omega)} \leq M$  a.e., hence  $v \in K$ .  $\square$

We now verify the compactness and continuity properties needed for Schauder’s fixed point theorem.

**Lemma 3.11.** *The map  $T : K \rightarrow X$  is compact (i.e.  $T(K)$  is relatively compact in  $X$ ).*

*Proof.* Fix  $u \in K$  and write  $v = T(u)$ . For each  $i$ ,  $v_i$  solves

$$-\Delta v_i + \frac{q_i}{\varepsilon} v_i = 0, \quad v_i|_{\partial\Omega} = \phi_i, \quad q_i := (u_j u_\ell)^2.$$

Since  $0 \leq u_j, u_\ell \leq M$ , we have  $0 \leq q_i \leq M^4$  a.e. Hence Lemma 3.3 gives

$$\|v_i\|_{H^1(\Omega)} \leq C(\Omega) \left(1 + \frac{M^4}{\varepsilon}\right) \|\phi_i\|_{H^{1/2}(\partial\Omega)}.$$

Thus  $T(K)$  is bounded in  $(H^1(\Omega))^3$ . By the Rellich–Kondrachov theorem, the embedding  $H^1(\Omega) \hookrightarrow L^2(\Omega)$  is compact, so  $T(K)$  is relatively compact in  $X$ .  $\square$

**Lemma 3.12.** *The map  $T : K \rightarrow X$  is continuous.*

*Proof.* Let  $u^{(m)} \rightarrow u$  in  $X$  with  $u^{(m)}, u \in K$ , and set  $v^{(m)} = T(u^{(m)})$ ,  $v = T(u)$ . Fix  $i$  and denote

$$q^{(m)} := (u_j^{(m)} u_\ell^{(m)})^2, \quad q := (u_j u_\ell)^2.$$

Using (13) and  $0 \leq u_r^{(m)}, u_r \leq M$ , yields

$$\|q^{(m)} - q\|_{L^2} \leq 2M^3 (\|u_j^{(m)} - u_j\|_{L^2} + \|u_\ell^{(m)} - u_\ell\|_{L^2}) \rightarrow 0.$$

Let  $w^{(m)} := v_i^{(m)} - v_i \in H_0^1(\Omega)$ . Subtracting the equations gives

$$-\Delta w^{(m)} + \frac{q^{(m)}}{\varepsilon} w^{(m)} = \frac{q - q^{(m)}}{\varepsilon} v_i \quad \text{in } \Omega, \quad w^{(m)}|_{\partial\Omega} = 0.$$

By Lemma 3.6 and  $0 \leq v_i \leq M$  (Lemma 3.10), we get

$$\|w^{(m)}\|_{L^2} \leq \frac{1}{\lambda_D} \left\| \frac{q - q^{(m)}}{\varepsilon} v_i \right\|_{L^2} \leq \frac{M}{\varepsilon \lambda_D} \|q^{(m)} - q\|_{L^2} \rightarrow 0.$$

Thus  $v_i^{(m)} \rightarrow v_i$  in  $L^2$ . Taking the maximum over  $i$  yields  $v^{(m)} \rightarrow v$  in  $X$ .  $\square$

The next lemma provides a global Lipschitz estimate for the Picard map  $T$  in  $X$ . It also records an interior improvement on compact sets whenever the competing pair  $(v_j v_\ell)^2$  stays uniformly positive in a neighborhood.

**Lemma 3.13.** *On above defined set  $K$ , the map  $T$  is Lipschitz, i.e.*

$$\|T(u) - T(v)\|_X \leq L_T \|u - v\|_X, \quad L_T := \frac{4M^4}{\varepsilon \lambda_D}.$$

Moreover, fix a compact set  $K_0 \Subset \Omega$  and an open neighborhood  $U \Subset \Omega$  of  $K_0$ . If for some index  $i \in \{1, 2, 3\}$  there exists  $\delta > 0$  such that

$$(v_j v_\ell)^2 \geq \delta \quad \text{a.e. in } U, \quad \{i, j, \ell\} = \{1, 2, 3\},$$

then there exist constants  $C = C(\Omega, U, K_0) > 0$  and  $c = c(\Omega, U, K_0) > 0$  such that

$$\|T(u)_i - T(v)_i\|_{L^2(K_0)} \leq C \frac{4M^4}{\varepsilon \lambda_D} \exp\left(-c \sqrt{\frac{\delta}{\varepsilon}}\right) \|u - v\|_X.$$

*Proof.* Fix  $i$  and write  $U := T(u)_i$ ,  $V := T(v)_i$ . Let  $q_u := (u_j u_\ell)^2$  and  $q_v := (v_j v_\ell)^2$ . Set  $w := U - V \in H_0^1(\Omega)$ . Subtracting gives

$$-\Delta w + \frac{q_u}{\varepsilon} w = \frac{q_v - q_u}{\varepsilon} V \quad \text{in } \Omega.$$

Lemma 3.6 yields

$$\|w\|_{L^2(\Omega)} \leq \frac{1}{\lambda_D} \left\| \frac{q_v - q_u}{\varepsilon} V \right\|_{L^2(\Omega)} \leq \frac{M}{\varepsilon \lambda_D} \|q_v - q_u\|_{L^2(\Omega)}.$$

Using (13) and  $0 \leq u_r, v_r \leq M$ , implies

$$\|q_v - q_u\|_{L^2} = \|(v_j v_\ell)^2 - (u_j u_\ell)^2\|_{L^2} \leq 2M^3 (\|u_j - v_j\|_{L^2} + \|u_\ell - v_\ell\|_{L^2}) \leq 4M^3 \|u - v\|_X.$$

Hence  $\|U - V\|_{L^2(\Omega)} \leq \frac{4M^4}{\varepsilon \lambda_D} \|u - v\|_X$ . Taking the maximum over  $i$  proves the global claim.

For the interior improvement, assume  $q_v \geq \delta$  a.e. in  $U$ . Then  $V$  solves  $-\Delta V + \frac{q_v}{\varepsilon} V = 0$  in  $\Omega$  with boundary trace  $\phi_i$ . By Lemma 3.7 we obtain

$$\|V\|_{L^\infty(K_0)} \leq C_0 \|\phi_i\|_{L^\infty(\partial\Omega)} \exp\left(-c_0 \sqrt{\frac{\delta}{\varepsilon}}\right) \leq C_0 M \exp\left(-c_0 \sqrt{\frac{\delta}{\varepsilon}}\right).$$

Using this exponential smallness on  $K_0$  yields the stated bound after absorbing constants into  $C, c$ .  $\square$

**Remark 3.14.** In Lemma 3.13, the interior factor  $\exp(-c\sqrt{\delta/\varepsilon})$  is small as  $\varepsilon \downarrow 0$  precisely when  $\delta/\varepsilon \rightarrow +\infty$ . More generally, if the lower bound is allowed to depend on  $\varepsilon$ ,

$$(v_j v_\ell)^2 \geq \delta_\varepsilon \quad \text{a.e. on } U,$$

then the same argument yields the interior factor  $\exp(-c\sqrt{\delta_\varepsilon/\varepsilon})$ . Consequently, if  $\delta_\varepsilon = O(\varepsilon)$ , the exponential factor remains bounded away from 0 as  $\varepsilon \downarrow 0$ , and no  $\varepsilon$ -driven improvement is obtained from this mechanism.

**Remark 3.15.** The global constant  $L_T = \frac{4M^4}{\varepsilon\lambda_D}$  in Lemma 3.13 is obtained by a worst-case bound using only  $0 \leq u_i \leq M$ . In the strong-competition regime  $\varepsilon \downarrow 0$  for variationally selected families, Lemmas 3.7 and 3.8 provide two additional interior mechanisms on compact sets  $K_0 \Subset \Omega$ . Lemma 3.7 yields exponential suppression of  $u_i^\varepsilon$  in regions where the “potential”  $q_i^\varepsilon := (u_j^\varepsilon u_\ell^\varepsilon)^2$  is bounded below away from 0. Lemma 3.8 shows that the weighted ternary interaction energy  $\int_{K_0} \varepsilon^{-1} (u_1^\varepsilon u_2^\varepsilon u_3^\varepsilon)^2 dx$  vanishes along a subsequence.

These two facts allow one to refine interior estimates beyond the global  $L^\infty$ -based bounds when  $\varepsilon$  is small.

The next lemma establishes a Lipschitz estimate for the Gauss–Seidel map  $G$  in  $X$ , together with an interior exponential improvement under a local lower bound on the corresponding Gauss–Seidel coefficient.

**Lemma 3.16.** *On  $K$ , the map  $G$  is Lipschitz:*

$$\|G(u) - G(v)\|_X \leq L_G \|u - v\|_X, \quad L_G := K(2 + 14K + 8K^2), \quad K := \frac{M^4}{\varepsilon\lambda_D}.$$

Moreover, fix  $K_0 \Subset \Omega$  and an open neighborhood  $U \Subset \Omega$  of  $K_0$ . Let  $a := G(u)$  and  $b := G(v)$ , and set  $d_i := a_i - b_i$ . If, for some  $\delta > 0$ , one of the following lower bounds holds a.e. in  $U$ :

$$\begin{aligned} (b1) \quad & (v_2 v_3)^2 \geq \delta, \\ (b2) \quad & \frac{1}{2} v_3^2 (v_1^2 + b_1^2) \geq \delta, \\ (b3) \quad & \frac{1}{2} ((v_1 v_2)^2 + (b_1 b_2)^2) \geq \delta, \end{aligned}$$

then there exist constants  $C = C(\Omega, U, K_0) > 0$  and  $c = c(\Omega, U, K_0) > 0$  such that, respectively,

$$\|d_1\|_{L^2(K_0)} \leq C(4K) e^{-c\sqrt{\delta/\varepsilon}} \|u - v\|_X, \quad \|d_2\|_{L^2(K_0)} \leq C K(3 + 4K) e^{-c\sqrt{\delta/\varepsilon}} \|u - v\|_X,$$

$$\|d_3\|_{L^2(K_0)} \leq C K(2 + 14K + 8K^2) e^{-c\sqrt{\delta/\varepsilon}} \|u - v\|_X.$$

*Proof.* Let  $a = G(u)$  and  $b = G(v)$ , and set  $d_r := a_r - b_r$ . The first GS step has the same structure as in Lemma 3.13. Therefore

$$\|d_1\|_{L^2(\Omega)} \leq 4K \|u - v\|_X.$$

Let

$$c_u := \frac{1}{2} u_3^2 (u_1^2 + a_1^2), \quad c_v := \frac{1}{2} v_3^2 (v_1^2 + b_1^2).$$

Then  $d_2 \in H_0^1(\Omega)$  solves

$$-\Delta d_2 + \frac{c_u}{\varepsilon} d_2 = \frac{c_v - c_u}{\varepsilon} b_2.$$

By Lemma 3.6 and  $0 \leq b_2 \leq M$ , we have

$$\|d_2\|_{L^2(\Omega)} \leq \frac{M}{\varepsilon\lambda_D} \|c_v - c_u\|_{L^2(\Omega)}.$$

Using (13) repeatedly and  $0 \leq (\cdot) \leq M$ , yields

$$\|c_v - c_u\|_{L^2(\Omega)} \leq M^3(3\|u - v\|_X + \|d_1\|_{L^2(\Omega)}).$$

Hence

$$\|d_2\|_{L^2(\Omega)} \leq K(3\|u - v\|_X + \|d_1\|_{L^2(\Omega)}) \leq K(3 + 4K)\|u - v\|_X.$$

Let

$$e_u := \frac{1}{2}((u_1 u_2)^2 + (a_1 a_2)^2), \quad e_v := \frac{1}{2}((v_1 v_2)^2 + (b_1 b_2)^2).$$

Then  $d_3 \in H_0^1(\Omega)$  solves

$$-\Delta d_3 + \frac{e_u}{\varepsilon} d_3 = \frac{e_v - e_u}{\varepsilon} b_3,$$

so by Lemma 3.6 and  $0 \leq b_3 \leq M$ , we get

$$\|d_3\|_{L^2(\Omega)} \leq \frac{M}{\varepsilon \lambda_D} \|e_v - e_u\|_{L^2(\Omega)}.$$

By (13), we have

$$\|e_v - e_u\|_{L^2(\Omega)} \leq 2M^3\|u - v\|_X + 2M^3(\|d_1\|_{L^2(\Omega)} + \|d_2\|_{L^2(\Omega)}),$$

hence

$$\|d_3\|_{L^2(\Omega)} \leq K(2\|u - v\|_X + 2\|d_1\|_{L^2(\Omega)} + 2\|d_2\|_{L^2(\Omega)}) \leq K(2 + 14K + 8K^2)\|u - v\|_X.$$

Taking the maximum over  $r = 1, 2, 3$  yields the Lipschitz constant  $L_G$ .

Assume one of (b1) – (b3) holds, and let  $q_r$  denote the corresponding coefficient in the  $r$ -th GS step. Then  $b_r$  solves

$$-\Delta b_r + \frac{q_r}{\varepsilon} b_r = 0 \quad \text{in } \Omega, \quad b_r|_{\partial\Omega} = \phi_r.$$

If  $q_r \geq \delta$  a.e. in a neighborhood  $U$  of  $K_0$ , Lemma 3.7 yields

$$\|b_r\|_{L^\infty(K_0)} \leq C_0 M \exp\left(-c_0 \sqrt{\frac{\delta}{\varepsilon}}\right), \tag{13}$$

for constants  $C_0, c_0$  depending only on  $(\Omega, U, K_0)$ . Combining (13) with the coefficient-difference bounds from Steps 1–3 gives the stated interior estimates after absorbing constants into  $C, c$ .  $\square$

---

**Algorithm 1** Monotone Iterative Scheme
 

---

- 1: **Initialize:** Compute harmonic extensions  $u_1^0, u_2^0, u_3^0$  satisfying the given boundary conditions.
- 2: **for**  $k = 0, 1, 2, \dots$  until convergence **do**
- 3:     **Update**  $u_1^{k+1}, u_2^{k+1}, u_3^{k+1}$  **from linear equations:**

$$\Delta u_1^{k+1/2} = \frac{u_1^{k+1/2}}{\varepsilon} (u_2^k u_3^k)^2, \quad u_1^{k+1/2}|_{\partial\Omega} = \varphi_1 \quad (20a)$$

$$u_1^{k+1} = \alpha u_1^{k+1/2} + (1 - \alpha) u_1^k \quad (20b)$$

$$\Delta u_2^{k+1/2} = \frac{u_2^{k+1/2}}{\varepsilon} (u_1^k u_3^k)^2, \quad u_2^{k+1/2}|_{\partial\Omega} = \varphi_2 \quad (20c)$$

$$u_2^{k+1} = \alpha u_2^{k+1/2} + (1 - \alpha) u_2^k \quad (20d)$$

$$\Delta u_3^{k+1/2} = \frac{u_3^{k+1/2}}{\varepsilon} (u_1^k u_2^k)^2, \quad u_3^{k+1/2}|_{\partial\Omega} = \varphi_3 \quad (20e)$$

$$u_3^{k+1} = \alpha u_3^{k+1/2} + (1 - \alpha) u_3^k \quad (20f)$$

- 4:     **Check convergence:** Stop if  $\|u_i^{k+1} - u_i^k\|_{L^2} < \text{tolerance}$  for all  $i$ .
  - 5: **end for**
- 

**Remark 3.17.** The following semi-implicit modification of Algorithm 1 achieves faster convergence by symmetrizing the coupling terms. Only the update equations for  $u_i^{k+1}$  are altered as follows:

$$\Delta u_1^{k+1} = \frac{u_1^{k+1}}{\varepsilon} (u_2^k u_3^k)^2, \quad (21a)$$

$$\Delta u_2^{k+1} = \frac{u_2^{k+1}}{\varepsilon} \frac{(u_1^k)^2 + (u_1^{k+1})^2}{2} (u_3^k)^2, \quad (21b)$$

$$\Delta u_3^{k+1} = \frac{u_3^{k+1}}{\varepsilon} \frac{(u_1^k u_2^k)^2 + (u_1^{k+1} u_2^{k+1})^2}{2}. \quad (21c)$$

The initialization and convergence criteria remain identical to those in Algorithm 1.

Another possible iterative scheme for fixed  $\varepsilon$  (with projection onto non-negativity) is:

$$-\Delta u_i^{k+1} + \frac{1}{2\varepsilon} u_i^{k+1} \left( \prod_{j \neq i} u_j^k \right)^2 = -\frac{1}{2\varepsilon} u_i^k \left( \prod_{j \neq i} u_j^k \right)^2 \quad \text{in } \Omega, \quad (22)$$

with  $u_i^{k+1} = \phi_i$  on  $\partial\Omega$  and the pointwise projection  $u_i^{k+1} = \max\{0, u_i^{k+1}\}$  to enforce non-negativity.

**Remark 3.18** (Implementation details). Let  $u_i \in \mathbb{R}^N$  be the nodal vector of  $u_i$  on a uniform grid, with indices partitioned into interior ( $I$ ) and boundary ( $B$ ) nodes such that

$$u_i = \begin{bmatrix} u_{i,I} \\ g_{i,B} \end{bmatrix}, \quad u_{i,B} = g_{i,B}.$$

Let  $K \in \mathbb{R}^{N \times N}$  and  $M \in \mathbb{R}^{N \times N}$  denote the consistent (FE) stiffness and mass matrices or (FD) analogues, both scaled by the grid spacings  $h_x, h_y$ . Both matrices are symmetric;  $M$  is positive definite and  $K$  is positive semidefinite. We use the block partitions

$$K = \begin{bmatrix} K_{II} & K_{IB} \\ K_{BI} & K_{BB} \end{bmatrix}, \quad M = \begin{bmatrix} M_{II} & M_{IB} \\ M_{BI} & M_{BB} \end{bmatrix}.$$

For a nonnegative nodal weight  $w \in \mathbb{R}^N$ , define

$$W = \text{diag}(w), \quad M(w) = W^{1/2} M W^{1/2} = \begin{bmatrix} M_{II}(w) & M_{IB}(w) \\ M_{BI}(w) & M_{BB}(w) \end{bmatrix}.$$

We introduce the variable weights

$$w_1 = (u_2 u_3)^2, \quad w_2 = (u_1 u_3)^2, \quad w_3 = (u_1 u_2)^2. \quad (23)$$

Then, the Dirichlet (gradient) and penalty parts are approximated for  $i = 1, 2, 3$  by quadratic forms as

$$\begin{aligned} \int_{\Omega} |\nabla u_i|^2 dx &\approx u_i^\top K u_i \\ &= u_{i,I}^\top K_{II} u_{i,I} + 2 g_{i,B}^\top K_{BI} u_{i,I} + g_{i,B}^\top K_{BB} g_{i,B}, \\ \int_{\Omega} (u_1 u_2 u_3)^2 dx &\approx u_i^\top M(w_i) u_i \\ &= u_{i,I}^\top M_{II}(w_i) u_{i,I} + 2 g_{i,B}^\top M_{BI}(w_i) u_{i,I} + g_{i,B}^\top M_{BB}(w_i) g_{i,B}. \end{aligned}$$

The  $k$ -th outer iterations of Algorithm 1 corresponds to solving the (constrained) full system

$$\left(K + \frac{1}{\varepsilon} M(w_i^k)\right) u_i^{k+1} = 0, \quad (u_i^{k+1})_B = g_{i,B} \quad (24)$$

for  $i = 1, 2, 3$ . Equivalently, the interior unknowns solve the reduced system

$$\left(K_{II} + \frac{1}{\varepsilon} M_{II}(w_i^k)\right) u_{i,I}^{k+1} = -K_{IB} g_{i,B} - \frac{1}{\varepsilon} M_{IB}(w_i^k) g_{i,B}. \quad (25)$$

Clearly, harmonic extensions in the initialization of Algorithm 1 solve the reduced system

$$(K_{II}) u_{i,I}^{k+1} = -K_{IB} g_{i,B}. \quad (26)$$

Both reduced linear systems for  $i = 1, 2, 3$  are symmetric and positive definite. Let us recall that for an  $N$ -point discretization, a multigrid-preconditioned iterative solution of (25) costs  $O(N \log N)$ , yielding  $O(mN \log N)$  per outer iterations with  $m = 3$ . The number of outer iterations grows like  $O(|\log \varepsilon|)$  as  $\varepsilon \rightarrow 0$ .

**3.2. Projected Gradient Method.** Let  $\mathbf{v} = (v_1, v_2, v_3) \in L^2(\Omega)^3$  and define the nonnegative parts  $s_i(x) = (v_i(x))^+ = \max\{v_i(x), 0\}$  for a.e.  $x \in \Omega$ ,  $i = 1, 2, 3$ . Let  $\mathcal{S} = \{(a_1, a_2, a_3) \in \mathbb{R}^3 : a_i \geq 0, a_1 a_2 a_3 = 0\}$  and write  $\mathcal{S} = \mathcal{S}_1 \cup \mathcal{S}_2 \cup \mathcal{S}_3$ , where  $\mathcal{S}_k = \{(a_1, a_2, a_3) \in \mathbb{R}^3 : a_i \geq 0, a_k = 0\}$  for  $k = 1, 2, 3$ . For  $\mathbf{v} = (v_1, v_2, v_3) \in L^2(\Omega)^3$ , define the map  $\mathcal{P} : L^2(\Omega)^3 \rightarrow L^2(\Omega)^3$  pointwise as follows. At each  $x \in \Omega$ , let

$$k^*(x) := \arg \min_{k \in \{1, 2, 3\}} (v_k(x))^+,$$

where  $(v)^+ = \max\{v, 0\}$ , with ties broken by selecting the smallest index. Set

$$(\mathcal{P}\mathbf{v})_i(x) = \begin{cases} (v_i(x))^+ & \text{if } i \neq k^*(x), \\ 0 & \text{if } i = k^*(x). \end{cases}$$

For boundary points  $x \in \partial\Omega$ , we simply set

$$s_i(x) = \varphi_i(x), \quad i = 1, 2, 3.$$

The following lemma shows why  $\mathcal{P}$  is indeed a projection.

**Lemma 3.19.** *Let  $\mathcal{P}\mathbf{v}(x)$  be defined as above. Then  $\mathcal{P}\mathbf{v}(x) \in \mathcal{S}$  for a.e.  $x \in \Omega$ , and  $\mathcal{P}\mathbf{v}$  is the  $L^2(\Omega)^3$ -metric projection of  $\mathbf{v}$  onto the admissible set, i.e.,*

$$\|\mathbf{v} - \mathcal{P}\mathbf{v}\|_{L^2(\Omega)^3}^2 = \min\{\|\mathbf{v} - \mathbf{w}\|_{L^2(\Omega)^3}^2 : \mathbf{w} \in L^2(\Omega)^3, \mathbf{w}(x) \in \mathcal{S} \text{ a.e.}\}.$$

*Proof.* Since the  $L^2(\Omega)^3$ -norm decouples as an integral of pointwise  $\ell^2$ -norms,

$$\|\mathbf{v} - \mathbf{w}\|_{L^2(\Omega)^3}^2 = \int_{\Omega} \|\mathbf{v}(x) - \mathbf{w}(x)\|_{\ell^2}^2 dx,$$

the global minimization reduces to solving, independently at each  $x \in \Omega$ , the finite-dimensional problem

$$\min_{\mathbf{y} \in \mathcal{S}} \|\mathbf{v}(x) - \mathbf{y}\|_{\ell^2}^2. \quad (27)$$

It therefore suffices to solve (27) for a fixed  $x$  and verify that  $\mathcal{P}\mathbf{v}(x)$  is optimal. Each face  $\mathcal{S}_k = \{\mathbf{y} \in \mathbb{R}^3 : y_i \geq 0, y_k = 0\}$  is a closed convex cone, so its Euclidean projection is given explicitly by  $\pi_k(\mathbf{v}(x)) = ((v_1(x))^+, (v_2(x))^+, (v_3(x))^+)$  with the  $k$ -th entry replaced by 0, i.e.

$$\pi_k(\mathbf{v}(x))_i = \begin{cases} 0 & \text{if } i = k, \\ \max\{v_i(x), 0\} = (v_i(x))^+ & \text{if } i \neq k. \end{cases}$$

The corresponding squared distance will be

$$\begin{aligned} d_k^2(x) &:= \|\mathbf{v}(x) - \pi_k(\mathbf{v}(x))\|_{\ell^2}^2 = \sum_{i=1}^3 |v_i(x) - \pi_k(\mathbf{v}(x))_i|^2 = \\ &= |v_k(x) - 0|^2 + \sum_{i \neq k} |v_i(x) - (v_i(x))^+|^2 = ((v_k(x))^+)^2 + \sum_{i=1}^3 ((v_i(x))^-)^2. \end{aligned} \quad (28)$$

where  $(v)^- = \max\{-v, 0\}$ .

Since  $\mathcal{S} = \mathcal{S}_1 \cup \mathcal{S}_2 \cup \mathcal{S}_3$  and each face is closed and convex, the projection onto the union is obtained by comparing the three candidates:

$$\min_{\mathbf{y} \in \mathcal{S}} \|\mathbf{v}(x) - \mathbf{y}\|_{\ell^2}^2 = \min_{k \in \{1,2,3\}} d_k^2(x).$$

Writing  $N(x) := \sum_{i=1}^3 ((v_i(x))^-)^2$ , expression (28) becomes  $d_k^2(x) = ((v_k(x))^+)^2 + N(x)$ . Because  $N(x)$  is common to all three faces, minimizing  $d_k^2(x)$  over  $k$  is equivalent to minimizing  $((v_k(x))^+)^2$ . The optimal face is therefore

$$k^*(x) = \arg \min_{k \in \{1,2,3\}} ((v_k(x))^+)^2 = \arg \min_{k \in \{1,2,3\}} (v_k(x))^+,$$

and the projection onto  $\mathcal{S}$  at  $x$  is  $\pi_{k^*(x)}(\mathbf{v}(x))$ , which sets the  $k^*$ -th component to zero and truncates the remaining two to their positive parts. This is precisely the map  $\mathcal{P}\mathbf{v}(x)$ .

By construction,  $(\mathcal{P}\mathbf{v}(x))_{k^*} = 0$  and  $(\mathcal{P}\mathbf{v}(x))_i \geq 0$  for  $i \neq k^*$ , so  $\mathcal{P}\mathbf{v}(x) \in \mathcal{S}_{k^*} \subset \mathcal{S}$  for a.e.  $x$ . Since  $\mathcal{P}\mathbf{v}(x)$  solves the pointwise problem (27) at a.e.  $x$ , integrating over  $\Omega$  yields

$$\|\mathbf{v} - \mathcal{P}\mathbf{v}\|_{L^2(\Omega)^3}^2 \leq \|\mathbf{v} - \mathbf{w}\|_{L^2(\Omega)^3}^2$$

for every  $\mathbf{w} \in L^2(\Omega)^3$  with  $\mathbf{w}(x) \in \mathcal{S}$  a.e. Finally, the index map  $x \mapsto k^*(x)$  is measurable because each  $(v_k)^+$  is measurable and the tie-breaking rule selects  $k^*$  as a measurable function of  $((v_1)^+, (v_2)^+, (v_3)^+)$ , whence  $\mathcal{P}\mathbf{v} \in L^2(\Omega)^3$ .  $\square$

---

### Algorithm 2 Projected Gradient Method

---

- 1: **Initialize:**  $(u_1^0, u_2^0, u_3^0) \in \mathcal{S}$  (e.g., harmonic extensions)
  - 2: Choose step size  $\alpha > 0$  (e.g.,  $\alpha = 0.1h^2$  for grid spacing  $h$ )
  - 3: **for**  $k = 0, 1, 2, \dots$  until convergence **do**
  - 4:     **for**  $i = 1, 2, 3$  **do**
  - 5:         Compute  $g_i^k = -Au_i^k$  ( $A$  discrete negative Laplacian)
  - 6:         Gradient step:  $\tilde{u}_i^{k+1} = u_i^k - \alpha g_i^k$
  - 7:     **end for**
  - 8:     Project:  $(u_1^{k+1}, u_2^{k+1}, u_3^{k+1}) = \mathcal{P}(\tilde{u}_1^{k+1}, \tilde{u}_2^{k+1}, \tilde{u}_3^{k+1})$
  - 9:     Check: if  $\max_i \|u_i^{k+1} - u_i^k\|_{L^2} < \varepsilon$  then **break**
  - 10: **end for**
  - 11: **return**  $(u_1^{k+1}, u_2^{k+1}, u_3^{k+1})$
- 

The projection  $\mathcal{P}$  operates pointwise: at each  $x \in \Omega$ , we solve

$$\min_{y \in S} \|v(x) - y\|_{\ell^2}^2, \quad S = \{(a_1, a_2, a_3) : a_i \geq 0, a_1 a_2 a_3 = 0\}.$$

Since  $S = S_1 \cup S_2 \cup S_3$  where  $S_k = \{a_k = 0, a_i \geq 0\}$  are convex, the minimizer is found by comparing three Euclidean projections onto cones. The projection  $\mathcal{P}$  is uniquely defined except on a set of measure zero (where two or more  $v_i^+$  coincide). The tie-breaking rule makes  $\mathcal{P}$  measurable.

**Remark 3.20.** For stability, choose  $\alpha < \lambda_{\max}(A)^{-1}$  where  $\lambda_{\max}(A)$  is the largest eigenvalue of the stiffness matrix. For a uniform grid with spacing  $h$ ,  $\lambda_{\max}(A) \sim h^{-2}$ , so  $\alpha \lesssim h^2$  ensures stability.

For faster convergence, use Nesterov acceleration (FISTA):

---

**Algorithm 3** FISTA for Projected Gradient Method
 

---

**Require:** Same as Algorithm 2

**Ensure:** Solution  $(u_1, u_2, u_3) \in \mathcal{S}$

```

1: Initialize  $(u_1^0, u_2^0, u_3^0)$  as in Algorithm 2
2: Set  $(y_1^0, y_2^0, y_3^0) \leftarrow (u_1^0, u_2^0, u_3^0)$  and  $t_0 \leftarrow 1$ 
3: for  $k = 0, 1, 2, \dots, K_{\max} - 1$  do
4:   Step 1: Gradient at momentum point
5:   for  $i = 1, 2, 3$  do
6:      $g_i^k \leftarrow -\Delta y_i^k$ 
7:   end for
8:   Step 2: Gradient step and projection
9:   for  $i = 1, 2, 3$  do
10:     $\tilde{u}_i^{k+1} \leftarrow y_i^k - \alpha \cdot g_i^k$ 
11:   end for
12:    $(u_1^{k+1}, u_2^{k+1}, u_3^{k+1}) \leftarrow \mathcal{P}((\tilde{u}_1^{k+1}, \tilde{u}_2^{k+1}, \tilde{u}_3^{k+1}))$ 
13:   Step 3: Nesterov momentum update
14:    $t_{k+1} \leftarrow \frac{1 + \sqrt{1 + 4t_k^2}}{2}$ 
15:    $\beta_k \leftarrow \frac{t_k - 1}{t_{k+1}}$ 
16:   for  $i = 1, 2, 3$  do
17:     $y_i^{k+1} \leftarrow u_i^{k+1} + \beta_k(u_i^{k+1} - u_i^k)$  ▷ Momentum extrapolation
18:   end for
19:   Step 4: Check convergence
20:   if  $\max_i \|u_i^{k+1} - u_i^k\|_{L^2} < \varepsilon$  then
21:     break
22:   end if
23: end for
24: return  $(u_1^{k+1}, u_2^{k+1}, u_3^{k+1})$ 

```

---

The projection operator  $\mathcal{P}$  defined in Lemma 3.19 can be interpreted as the proximal operator of the indicator function  $I_{\mathcal{S}}$ :

$$\mathcal{P}(v) = \text{prox}_{\tau I_{\mathcal{S}}}(v) = \arg \min_{w \in \mathcal{S}} \|w - v\|_{L^2(\Omega)}^2.$$

This proximal splitting perspective provides a unifying theoretical framework. Algorithm 2 is forward-backward splitting. Algorithm 3 is accelerated forward-backward splitting. The projection decouples pointwise, making the proximal operator explicitly computable

This interpretation connects our methods to the broader literature on proximal algorithms for nonconvex problems.

**Remark 3.21.** The set  $S$  is nonconvex, and the Dirichlet energy restricted to  $S$  may admit multiple stationary points. Consequently, projected (and accelerated) gradient iterations are not guaranteed to converge to a global minimizer; they should be interpreted as heuristics seeking low-energy segregated configurations, potentially dependent on initialization and parameter choices.

#### 4. SIMULATIONS

**Example 4.1.** Let  $\Omega = [-1, 1] \times [-1, 1]$ . We compare the penalization method and the projected gradient method on a uniform Cartesian grid with spacing  $h = \Delta x = \Delta y = 0.005$ . For the penalization scheme, we take  $\varepsilon = 10^{-9}$ . The Dirichlet boundary data  $\phi_i$  on  $\partial\Omega$  are prescribed by

$$\phi_1 = \chi_{\{y < 0\}} |y|, \quad \phi_2 = \chi_{\{y > 0\}} |y|, \quad \phi_3 = 0.25.$$

In Figures 1–2 we report the penalized solution  $u_i^\varepsilon$  by surface plots for  $u_1^\varepsilon, u_2^\varepsilon, u_3^\varepsilon$ , together with a contour plot highlighting the segregation interfaces.

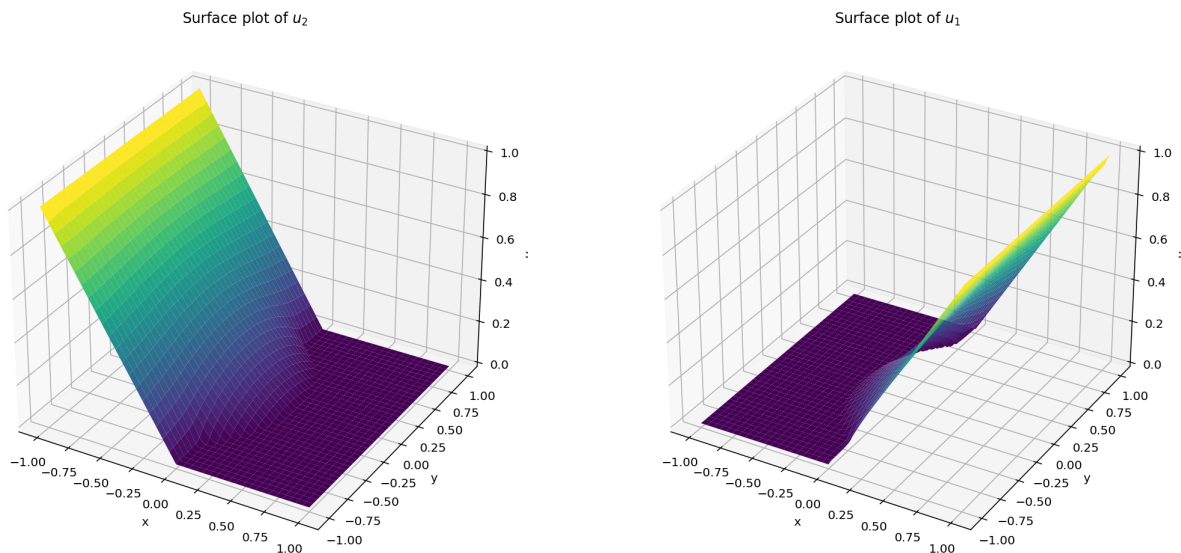


FIGURE 1. Surface plots of  $u_1^\varepsilon$  (left) and  $u_2^\varepsilon$  (right).

Figure 3 displays the output of the projected gradient method for the boundary data of Example 4.1. The top row shows filled contour plots of the three components  $u_1$ ,  $u_2$ , and  $u_3$  on  $\Omega = [-1, 1]^2$ , with the dashed rectangle indicating the inner square  $[-0.3, 0.3]^2$ . The contours of  $u_1$  and  $u_2$  confirm that these two components partition the domain into upper and lower half-regions, consistent with the imposed Dirichlet data  $\phi_1 = \chi_{\{y < 0\}} |y|$  and  $\phi_2 = \chi_{\{y > 0\}} |y|$ , while the third component  $u_3$  concentrates near the lateral boundary  $\{x = \pm 1\}$  and decays rapidly toward the interior. Inside the inner square,  $u_3$  is effectively zero (mean value  $\approx 0.0482$ , compared with the boundary prescription  $\phi_3 = 0.25$ ), indicating that the segregation constraint  $u_1 u_2 u_3 = 0$  forces  $u_3$  to vanish in the region where  $u_1$  and  $u_2$  are both appreciably positive. The bottom-left

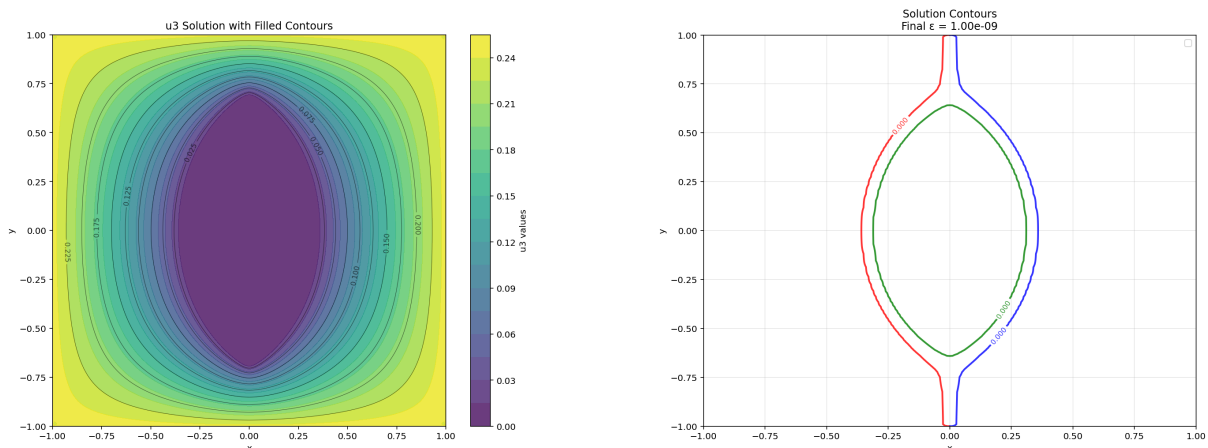


FIGURE 2. Surface plot of  $u_3^\varepsilon$  (left) and a  $\varepsilon$  contour(right) with penalization.

panel records the evolution of the discrete Dirichlet energy  $E_h(u^k)$  over the iteration history; the energy decreases monotonically over approximately 3500 iterations, stabilizing at a value consistent with the penalization result for the same boundary configuration. The bottom-center panel tracks the maximum pointwise constraint violation  $\max_{x \in \Omega_h} |u_1(x) u_2(x) u_3(x)|$ , which drops below  $10^{-10}$  within the first few hundred iterations and remains at machine-precision level thereafter, confirming that the projection step enforces the segregation constraint to full numerical accuracy at every iteration. Finally, the bottom-right panel compares the mean value of  $u_3$  in three subregions: the boundary layer (where  $\phi_3 = 0.25$ ), the inner square (where  $u_3 \approx 0$ ), and the outer annular region. The sharp contrast between the boundary value 0.25 and the interior mean 0.0482 quantifies the spatial extent of the segregation:  $u_3$  is driven to zero wherever  $u_1$  and  $u_2$  coexist, and retains significant values only in a narrow layer adjacent to  $\partial\Omega$  where the competing components are small.

**Example 4.2.** We illustrate the performance of the accelerated projected gradient method (FISTA) on the square domain  $\Omega = [-1, 1]^2$  discretized by a uniform Cartesian grid with mesh size  $h = \Delta x = \Delta y$ . The interface set is visualized as the union of the boundaries of the superlevel sets  $\{u_i > \delta\}$  (for a fixed small  $\delta > 0$ ).

**Boundary data.** We prescribe nine qualitatively distinct boundary configurations  $\{\phi_i\}_{i=1}^3$  on  $\partial\Omega$  as listed in Table 1. These configurations were introduced in [5] and provide a standard benchmark for three-phase segregation on a square.

**Initialization.** As an initial guess  $u^0 = (u_1^0, u_2^0, u_3^0)$  we employ the harmonic extension of the boundary data: for each  $i \in \{1, 2, 3\}$  we solve the discrete Laplace problem

$$\Delta_h u_i^0 = 0 \quad \text{in } \Omega_h, \quad u_i^0 = \phi_i \quad \text{on } \partial\Omega_h,$$

where  $\Omega_h$  denotes the set of interior grid points and  $\Delta_h$  is the standard five-point Laplacian. The resulting triple is then projected pointwise onto  $S$  to enforce nonnegativity and hard segregation.

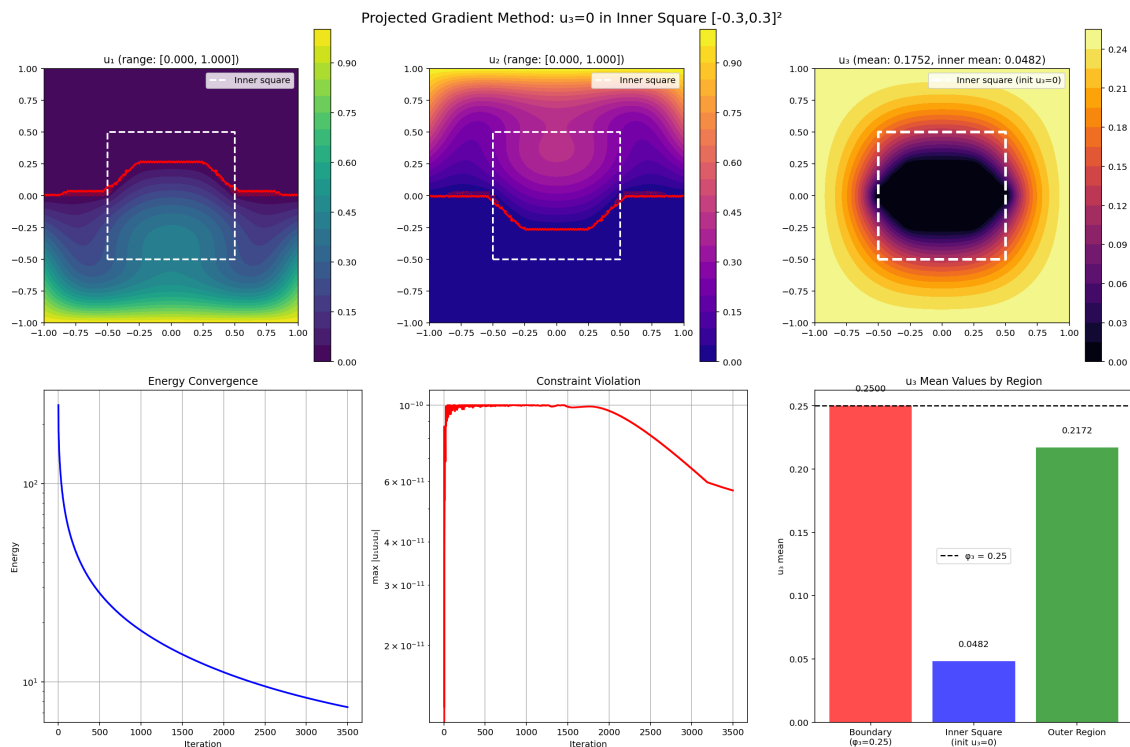


FIGURE 3. Projected gradient method for Example 4.1 on  $\Omega = [-1, 1]^2$ . Top row: filled contour plots of  $u_1$ ,  $u_2$ , and  $u_3$ ; the dashed rectangle marks the inner square  $[-0.3, 0.3]^2$ . Bottom row: energy convergence history (left), maximum constraint violation  $\max |u_1 u_2 u_3|$  (center), and mean values of  $u_3$  by region (right).

FISTA iteration with projection. Let  $u^k \in S$  denote the current iterate and define an extrapolated point

$$y^k = u^k + \beta_k (u^k - u^{k-1}), \quad \beta_k = \frac{t_{k-1} - 1}{t_k}, \quad t_k = \frac{1 + \sqrt{1 + 4t_{k-1}^2}}{2}, \quad t_0 = 1,$$

with the convention  $u^{-1} = u^0$ . Given a step size  $\alpha > 0$ , one FISTA step takes the form

$$\tilde{u}^{k+1} = y^k + \alpha \Delta_h y^k, \quad u^{k+1} = P_S(\tilde{u}^{k+1}),$$

where  $P_S$  denotes the pointwise projection onto  $S$  obtained by truncating negative values and setting, at each grid point, the smallest component to zero. Dirichlet data are enforced by resetting  $u^{k+1} = \phi$  on  $\partial\Omega_h$  after the projection.

Since the projection onto  $S$  is nonconvex, we incorporate standard safeguards to improve robustness across all boundary configurations: (i) a small “hysteresis” tolerance is used in the projection to avoid spurious phase switching at near-ties; (ii) a proximal bias may be applied prior to projection via  $\tilde{u}^{k+1} \leftarrow (\tilde{u}^{k+1} + \eta u^k)/(1 + \eta)$  with  $\eta \geq 0$ ; and (iii)  $\alpha$  is selected by

TABLE 1. Boundary conditions on  $\Omega = [-1, 1]^2$ , with  $\theta = \arctan(y/x)$ .

BC	Definition on $\partial\Omega$
1	$\phi_i = \max(0, \cos(\theta - 2\pi i/3))$ , $i = 1, 2, 3$
2	$\phi_i = \max(0, \cos(\theta - 2\pi i/3 - \pi/4))$ , $i = 1, 2, 3$
3	$\phi_1 _{y=-1} = 1$ ; $\phi_2 _{y=1} = 1$ ; $\phi_3 _{x=\pm 1} = 0.5$
4	$\phi_1 = x^+$ ; $\phi_2 = (-x)^+$ ; $\phi_3 = 0.25$
5	$\phi_1 _{y=\pm 1} = 1$ ; $\phi_2 _{x=\pm 1} = 1$ ; $\phi_3 = 0.3$
6	$\phi_i = \max(0, 1 -  z - c_i /2)$ ; $c_1 = (-1, -1)$ , $c_2 = (1, 1)$ , $c_3 = (1, -1)$
7	$\phi_1 _{y=\pm 1} = \sin \frac{\pi(x+1)}{2}$ ; $\phi_2 _{y=\pm 1} = \left(\cos \frac{\pi(x+1)}{2}\right)^+$ ; $\phi_3 _{x=\pm 1} = 0.3$
8	$\phi_1 _{y=-1, x<0} = 1$ ; $\phi_2 _{y=-1, x>0} = 1$ ; $\phi_3 _{y=1} = 1$
9	$\phi_1 _{y=-1 \cup x=-1} = 1$ ; $\phi_2 _{y=1 \cup x=1} = 1$ ; $\phi_3 = 0.2$

backtracking to ensure a monotone decrease of a Dirichlet-energy surrogate,

$$\mathcal{E}_h(u) = \frac{1}{2} \sum_{i=1}^3 \sum_{x \in \Omega_h} |\nabla_h u_i(x)|^2 h^2,$$

where  $\nabla_h$  is the standard finite-difference gradient. If the energy increases, we perform a FISTA restart by resetting  $t_k = 1$  and  $y^k = u^k$ .

Parameters and stopping criterion. We use a uniform grid with  $h = \Delta x = \Delta y = 0.01$  (i.e.,  $n = 201$  points per coordinate direction). The initial step size is chosen as  $\alpha_0 = 0.03 h^2 = 3 \times 10^{-6}$  with a backtracking lower bound  $\alpha_{\min} = 10^{-5} h^2 = 10^{-9}$  and shrink factor  $\rho = 0.5$ . In addition, we use a proximal bias parameter  $\eta = 0.2$  and a hysteresis tolerance  $\tau = 10^{-10}$  in the pointwise projection to stabilize phase selection near ties.

Figure 4 shows the corresponding numerical partition obtained by the projected gradient scheme under the same boundary data.

In both approaches, the computed solutions exhibit a clearly segregated configuration with sharp interfaces separating the active regions of the three components. In particular, the contour plots indicate that  $u_3$  concentrates near  $\partial\Omega$ , forming a boundary layer around the perimeter, while  $u_1$  and  $u_2$  dominate the lower and upper portions of the domain, respectively, in accordance with the imposed Dirichlet data. For the sake of comparison in Figure 5, we employ the penalization method for the same nine distinct boundary configurations listed in Table 1.

Figure 5 reports the segregation interfaces produced by Algorithm 1 for the nine boundary configurations listed in Table 1, computed on the uniform Cartesian grid with mesh size  $h = \Delta x = \Delta y = 0.004$  and penalization parameter  $\varepsilon = 10^{-9}$ . The free boundary  $\Gamma_i := \partial\{u_i > 0\}$  of each component is visualized as the level curve

$$\Gamma_i^\delta := \{x \in \Omega : u_i^\varepsilon(x) = \delta\}, \quad \delta = \sqrt{\varepsilon} = 10^{-5}, \quad (29)$$

and the three curves  $\Gamma_1^\delta$ ,  $\Gamma_2^\delta$ ,  $\Gamma_3^\delta$  are superimposed in red, blue, and green, respectively. The choice  $\delta = \sqrt{\varepsilon}$  is motivated by the decay rate of the penalized solution near the free boundary.

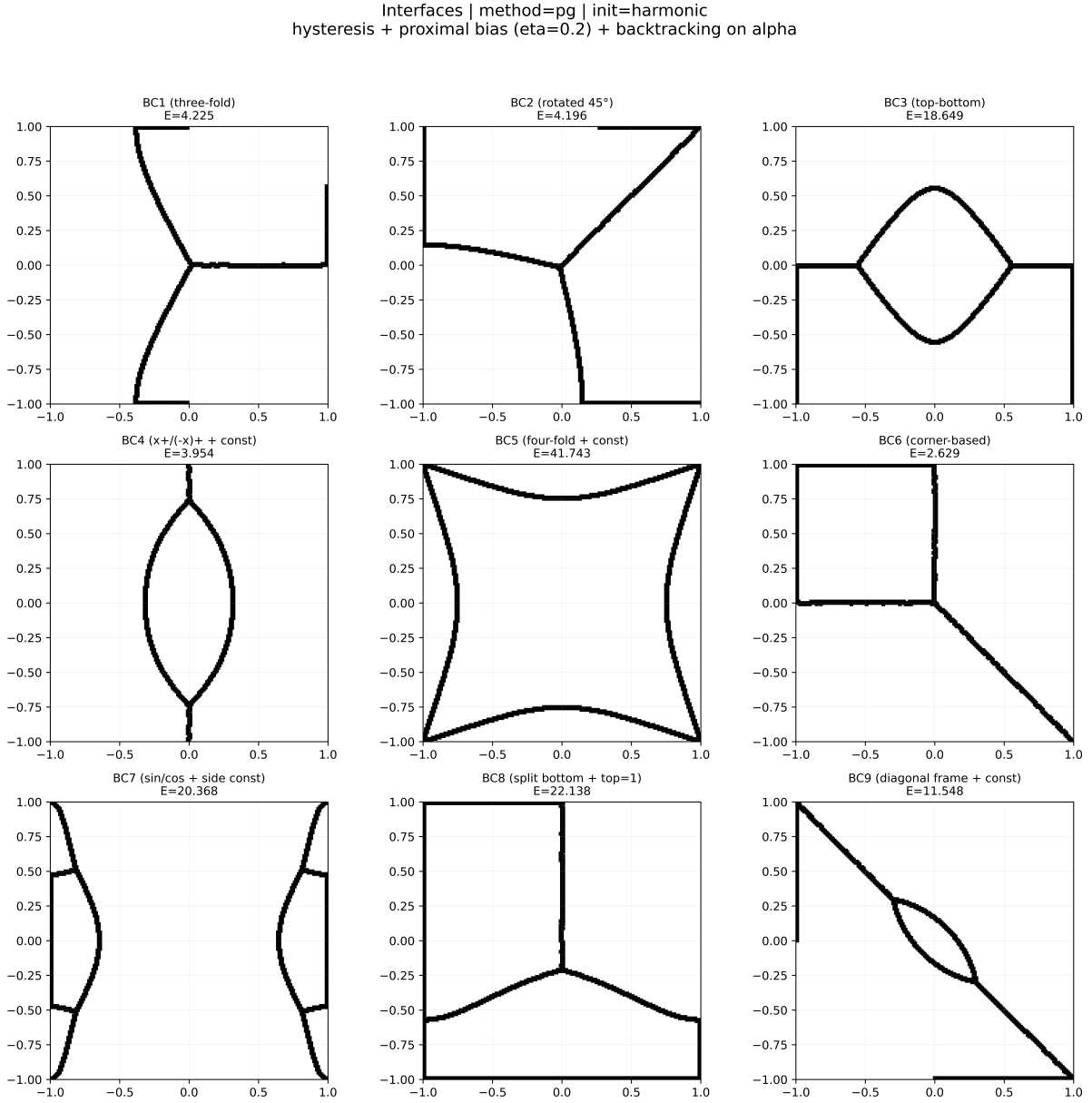


FIGURE 4. Gradient projected method on  $\Omega = [-1, 1]^2$ .

Across all nine boundary configurations, the computed interfaces are sharp, free of oscillations, and agree visually with those obtained by projected gradient and the direct construction method [5].

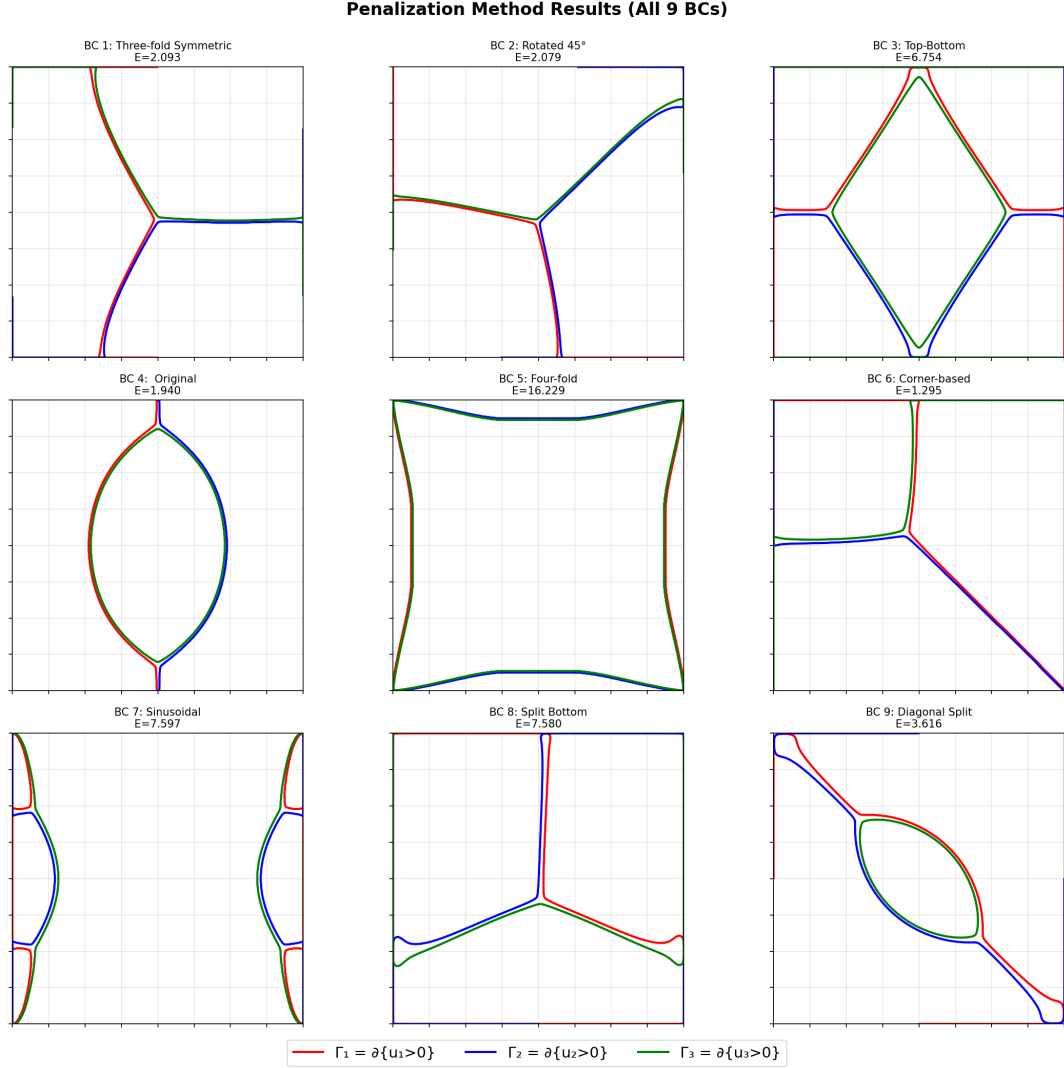


FIGURE 5. Penalization Method: segregation interfaces on  $\Omega = [-1, 1]^2$ .

## 5. CONCLUSION AND IMPACT

We investigated numerical algorithms for elliptic systems under partial segregation constraints, motivated by the need to compute segregated multi-phase configurations when classical constraint qualifications fail. Two complementary strategies were developed. The first is strong competition penalization combined with damped Gauss–Seidel/Picard iterations and  $\varepsilon$ -continuation, yielding robust segregated patterns as  $\varepsilon \rightarrow 0$ . The second is a projected gradient framework (with an accelerated variant, in the spirit of FISTA) relying on an explicit pointwise projection in the three-phase setting, which provides a simple and scalable alternative when coupled elliptic solves become expensive.

The main limitation is nonconvexity: both the feasible set and (depending on formulation) the effective objective may admit multiple stationary points, so computed configurations can depend on initialization and continuation schedules. In addition, the penalized formulation becomes increasingly stiff as  $\varepsilon$  decreases, suggesting that relaxation parameters and solver tolerances must scale with  $\varepsilon$  to maintain stability.

## REFERENCES

- [1] ARAKELYAN, A., AND SHAHGHOULIAN, H. Multi-phase quadrature domains and a related minimization problem. *Potential Analysis* 45, 1 (2016), 135–155.
- [2] BAINES, M. J., AND CHRISTOU, K. A moving-mesh finite-difference method for segregated two-phase competition-diffusion. *Mathematics* 9, 4 (2021), 386.
- [3] BARRETT, J. W., GARCKE, H., AND NÜRNBERG, R. Phase field models versus parametric front tracking methods: Are they accurate and computationally efficient? *Communications in Computational Physics* 15, 2 (February 2014), 506–555.
- [4] BOZORGNIA, F. Optimal partitions for first eigenvalues of the laplace operator. *Numerical Methods for Partial Differential Equations* 31, 3 (2015), 923–949.
- [5] BOZORGNIA, F. Identical free boundaries in two partially segregated systems. *arXiv preprint arXiv:2601.05682* (2026).
- [6] BOZORGNIA, F., AND ARAKELYAN, A. Gamma convergence of partially segregated elliptic systems. *arXiv preprint arXiv:2510.03794* (2025).
- [7] BOZORGNIA, F., BURGER, M., AND FOTOUHI, M. On a class of singularly perturbed elliptic systems with asymptotic phase segregation. *Discrete and Continuous Dynamical Systems* 42, 7 (2022), 3539–3556.
- [8] BUCUR, D., AND VELICHKOV, B. Multiphase shape optimization problems. *SIAM Journal on Control and Optimization* 52, 6 (2014), 3556–3591.
- [9] CAFFARELLI, L., KARAKHANYAN, A., AND LIN, F.-H. The geometry of solutions to a segregation problem for nondivergence systems. *Journal of Fixed Point Theory and Applications* 5, 2 (2009), 319–351.
- [10] CAFFARELLI, L. A., AND LIN, F.-H. Singularly perturbed elliptic systems and multi-valued harmonic functions with free boundaries. *Communications on Pure and Applied Mathematics* 60, 9 (2007), 1443–1487.
- [11] CHERNIHA, R., AND DAVYDOVYCH, V. New conditional symmetries and exact solutions of the diffusive two-component lotka–volterra system. *Mathematics* 9, 16 (2021), 1984.
- [12] CHERNIHA, R., AND DAVYDOVYCH, V. Construction and application of exact solutions of the diffusive lotka–volterra system: A review and new results. *Communications in Nonlinear Science and Numerical Simulation* 113 (2022), 106579.
- [13] CHERNIHA, R., AND KRIUKOVA, G. A reaction–diffusion system with nonconstant diffusion coefficients: Exact and numerical solutions. *Axioms* 14, 9 (2025), 655.
- [14] CONTI, M., TERRACINI, S., AND VERZINI, G. Asymptotic estimates for the spatial segregation of competitive systems. *Adv. Math.* 195, 2 (2005), 524–560.
- [15] CONTI, M., TERRACINI, S., AND VERZINI, G. A variational problem for the spatial segregation of reaction-diffusion systems. *Indiana Univ. Math. J.* 54, 3 (2005), 779–815.
- [16] CROOKS, E. C. M., DANCER, E. N., HILHORST, D., MIMURA, M., AND NINOMIYA, H. Spatial segregation limit of a competition-diffusion system with dirichlet boundary conditions. *Nonlinear Analysis: Real World Applications* 5, 4 (2004), 645–665.
- [17] EKELAND, I., AND TEMAM, R. *Convex Analysis and Variational Problems*. SIAM, Philadelphia, 1999.
- [18] ITO, K., AND KUNISCH, K. *Lagrange Multiplier Approach to Variational Problems and Applications*. SIAM, Philadelphia, 2008.
- [19] KANZOW, C., RAHARJA, A. B., AND SCHWARTZ, A. An augmented lagrangian method for cardinality-constrained optimization problems. *Journal of Optimization Theory and Applications* 189, 3 (2021), 793–813.
- [20] KAO, C.-Y., AND MOHAMMADI, S. A. Maximal total population of species in a diffusive logistic model. *Journal of Mathematical Biology* 85, 5 (2022), 47.

- [21] KAO, C.-Y., MOHAMMADI, S. A., AND YOUSEFNEZHAD, M. Is maximum tolerated dose (mtd) chemotherapy scheduling optimal for glioblastoma multiforme? *Communications in Nonlinear Science and Numerical Simulation* 139 (2024), 108292.
- [22] LIU, S., AND LIU, X. Numerical methods for a two-species competition-diffusion model with free boundaries. *Mathematics* 6, 5 (2018), 72.
- [23] MERRIMAN, B., BENCE, J. K., AND OSHER, S. J. Motion of multiple junctions: A level set approach. *Journal of Computational Physics* 112, 2 (1994), 334–363.
- [24] SOAVE, N., AND TERRACINI, S. The nodal set of solutions to some elliptic problems: sublinear equations, and competition–diffusion systems. *Advances in Mathematics* 279 (2015), 490–531.
- [25] SOAVE, N., AND TERRACINI, S. On partially segregated harmonic maps: optimal regularity and structure of the free boundary, 2024. arXiv preprint.
- [26] SOAVE, N., AND TERRACINI, S. On some singularly perturbed elliptic systems modeling partial segregation, part 1: uniform hölder estimates and basic properties of the limits, 2024. arXiv:2409.11976.
- [27] SQUASSINA, M. On the long term spatial segregation for a competition-diffusion system. *Asymptot. Anal.* 57, 1-2 (2008), 83–103.
- [28] SWAILEM, M., AND TÄUBER, U. C. Computing macroscopic reaction rates in reaction-diffusion systems using monte carlo simulations. *Physical Review E* 110, 1 (July 2024), 014124.
- [29] VERZINI, G., AND ZILIO, A. Strong competition versus fractional diffusion: the case of lotka–volterra interaction. *Communications in Partial Differential Equations* 39, 12 (2014), 2284–2313.
- [30] WACHSMUTH, G. Mathematical programs with complementarity constraints in Banach spaces. *Journal of Optimization Theory and Applications* 166, 2 (2015), 382–422.
- [31] WANG, K., AND ZHANG, Z. Some new results in competing systems with many species. *Annales de l’Institut Henri Poincaré C, Analyse Non Linéaire* 27, 2 (2010), 739–761.
- [32] WEI, J., AND WETH, T. Asymptotic behaviour of solutions of planar elliptic systems with strong competition. *Nonlinearity* 21, 2 (2008), 305–317.